JOURNAL OF MATERIALS SCIENCE 20 (1985) 3091 – 3100

Rapidly solidified aluminium–iron–misch metal alloys

A. K. GOGIA, P. V. RAO, J. A. SEKHAR
Defence Metallurgical Research Laboratory, P.O. Kanchanbagh, Hyderabad-500258, India

Three alloys with compositions of Al–10 Fe–1.25 MM (misch metal), Al–6.7 Fe–3.2 MM and Al–3.7 Fe–1.2 MM were rapidly solidified into strips. Four broad categories of as-cast microstructures could be identified in all microstructures with the volume fraction of a microstructure being dependent on the composition and thickness of the strip. Similarly, the amount of Al_3Fe, Al_6Fe, and Al_8CeFe_4 intermetallics also varied with composition in the as-cast condition. Lattice parameter measurement by X-ray diffraction indicated that the opposing influence of iron and atoms such as cerium keeps the distortion in the aluminium lattice to below 0.16% over that of pure aluminium. Heat treatment of the strips was carried out for temperatures up to 618 K and times up to 318 h to follow the changes occurring in the microstructure. These changes include coarsening of cells, precipitation and growth of intermetallics and cyclic changes in the measured microhardness values at different thickness locations in the strips.

1. Introduction

Rapid solidification processing of aluminium alloys can lead to significant improvements in mechanical properties in both the dispersion strengthened alloys and the precipitation strengthened alloys [1–12]. The complete processing to net shape involves (a) making the rapidly solidified alloy strip or powder, (b) consolidating the crushed strip or powder, and (c) the final thermomechanical treatment. Unlike in conventional wrought aluminium alloys, features of the microstructures of the rapidly cast dispersion strengthened material, if retained in the final microstructure after consolidation, will lead to beneficial strength properties. Furthermore, the sizes and morphology of the intermetallics in the solidified structures will influence the fracture toughness properties. It is therefore important to characterize the initial cast microstructure and to follow the changes caused by heat treatment.

The aim of this paper is to discuss such microstructures for three rapidly solidified strips of aluminium–iron–misch metal alloys. The alloys were made and studied with the intention of developing a high temperature stable (500 to 620 K) aluminium alloy. Aluminium alloys that have been studied with this goal contain iron, nickel, cobalt, cerium, molybdenum, oxygen manganese, silicon [4–6, 9, 12, 13] so that the microstructure may contain stable and closely spaced precipitates.

Rapid solidification of many aluminium alloys by the strip or splat making technique has been shown to normally contain at least two optically distinct zones. Initially observed by Jones [10] and later reported by others [5, 12, 14] these are (i) zone A which appears light in the optical microscope and forms in the material in contact with the copper substrate, and (ii) zone B which appears dark in the optical microscope and forms in regions of the strip away from the wheel. Zone A is harder [10] and is extremely fine cellular in a colony of grains. Zone B, which may

0022–2461/85 $03.00 + .12

be equiaxed dendritic [14], consists of coarser cells than those observed in zone A and shows the presence of interdendritic segregation as well as the presence of second phase particles. The average volume per cent of second phase increases with distance from the wheel and also with increasing ribbon thickness [14]. Reducing the Fe content in Al-Fe splats and an increased heat extraction rate leads to a greater fraction of zone A [10]. Similarly, transition from zone A to zone B proceeds across the strip with the appearance of the second phase and could be a transition from the near partitionless primary solidification obtained at high growth velocities in supercooled melts to normal partitional solidification in the two phase region (i.e. with the change in the partition coefficient and interface temperature). A coupled eutectic zone may be swept during the transition [10]. The transition is also somewhat abrupt either because of an abrupt solidification rate change [10, 15] and/or because of a well defined temperature for two-phase solidification. Furthermore, as postulated by Garrett and Sanders [16] primary nucleation of the coarse intermetallic may also limit the extent of zone A.

Decomposition during heat treatment of the rapidly solidified Al–Fe and Al–Fe–MM alloys involves the precipitation and/or growth of Al_6Fe, Al_3Fe and Al_8Fe_4Ce [4, 5, 16, 17]. Temperatures of the order of 617 K (0.66 T_m) were adequate for the precipitation of Al_3Fe [4]. Jones [17], however, reports a decomposition temperature as high as 0.9 T_m for Al–Cr and 0.67 T_m for Al–Zr. The precipitation temperature seems dependent on the ease of precipitation being possible on widely separated defects such as grain boundaries [17]. Growth of existing precipitates can occur at lower temperatures and is enhanced again by residence of the particles on grain boundaries [17]. Below 0.5 T_m the Al_6Fe evidently need not transform to Al_3Fe and can coarsen and grow [18]. The coarsening, however, is controlled by the existence of any Al_3Fe particles resident at the grain or cell boundaries [18, 19]. Jones [17] has also concluded that the greatest stability against decomposition is available through (i) a low solute diffusion in the matrix, and (ii) the existence of defects which are widely separated. For the Al–8 Fe and Al–8 Fe–(3% Mn or 1% Zr) zone B microstructure has been found to be more stable than zone A microstructure when heat treated between 573 and 673 K [9, 20].

TABLE I Composition of the three alloys (wt %)

	Alloy		
	I	II	III
Fe	10	6.7	3.7
MM	1.25	3.2	1.2

Trace: Si ~ 0.15, C ~ 0.04, O ~ 100 ppm

2. Experimental techniques

Three alloys were studied as listed in Table I. They were made by melting electrolytic iron and 99.5% pure aluminium in a 25 mm radius and 50 mm height clay graphite crucible. Misch metal (50 to 55 wt % Ce, 0.14 wt % Fe, 20 to 25 wt % La, 4 to 6 wt % Pr, 10 to 15 wt % Nd) was added to the liquid after degassing with commercial chlorine compounds. The strips were made as described previously [5, 21]. Liquid metal is ejected through a rectangular orifice on to a cold copper wheel with a surface velocity of 45 m sec^{-1}. The resultant strips from the planar flow casting machine were uneven and could vary between 50 and 80 μm thick. Occasionally in some areas the thickness of the strips in alloys I and II could even approach 170 μm. Continuous strips (0.03 m width) were obtained for alloys I and III whereas only split strips could be obtained for alloy II. The composition maxima of trace elements in the strip condition is also shown in the table. During heat treatment of the strips the temperature was monitored with a thermocouple in contact with the strips.

The strips were studied in the optical and transmission electron microscope. Thin foils for TEM were prepared by electropolishing (window technique) in an electrolyte of 20% $HClO_4$ and ethanol solution at $-30°$ C at 15 V. X-ray intensities were recorded by Co$K\alpha$ radiation and the peaks were determined by exposing both faces of the strip to radiation in a Phillips X-ray diffractometer. For the lattice constants determination, only the wheel contact face was exposed to radiation.

3. Results and discussion

Optical examination of the strips revealed two zones, A and B. Both zones could extend through the thickness. Although alloys I and III

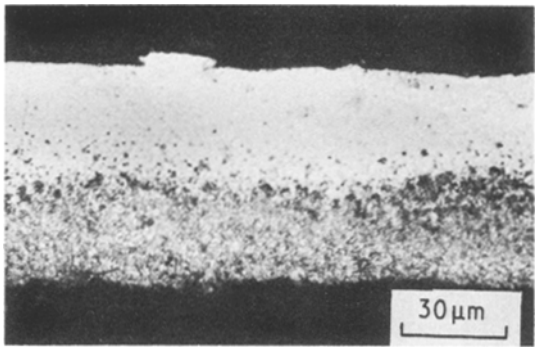

Figure 1 Optical micrograph of alloy II showing zones A and B. Al_3Fe needles are sometimes seen at the edge of zone B. (as-cast condition.)

show, on average, only about 10 to 30% of zone A, alloy II shows up to 50% of zone A as shown in Fig. 1. The amounts of the two zones varied over the length of the strip. The alloys were examined mostly in the TEM as described below and the microstructures reported in the as-solidified condition and after heat treatment are not directly correlated to the two zones. However, on many occasions it is deductively evident in which region the microstructure is being observed.

3.1. X-ray data

X-ray examination with Co$K\alpha$ radiation indicates that in the as-solidified condition alloy I contains Al_3Fe, Al_8CeFe_4 and an aluminium matrix with a lattice constant value of 0.4053 nm. After heat treatment at 618 K 312 h, Al_6Fe peaks are also additionally indicated. The observed d spacings and relative intensities are shown in Table II.

In the as-solidified condition, alloy II displayed no second phase lines and an aluminium lattice constant value of 0.405 nm was measured. After heat treating at 618 K/312 h, the Al_3Fe, Al_6Fe and Al_8CeFe_4 peaks were evident as recorded in Table III. In this alloy the Al_3Fe peaks appeared after a 503 K/168 h heat treatment. Alloy III in the as-solidified condition revealed Al_6Fe, Al_3Fe and an aluminium matrix with a lattice spacing of 0.4057 nm. Not much change was observed in the relative intensities at 373 K/318 h but only the Al_3Fe intermetallic peak (apart from matrix peaks) was indicated after the 618 K/312 h heat treatment. Table IV shows the d spacing and relative intensities for this alloy.

TABLE II X-ray diffraction data for alloy I

As-cast		Aged 345° C/312 h	
Observed d (nm)	Relative intensity	Observed d (nm)	Relative intensity
0.627*	2	0.627*	2
0.440*	2	0.486†	10
0.405‡	6	0.439†	7
0.395‡	5	0.427†	7
0.367‡	3	0.405‡	6
0.354‡	2	0.396‡	4
0.347‡	3	0.385‡	4
0.335‡	3	0.370†	6
0.326‡	3	0.362‡	3
0.238‡	3	0.346†	4
M 0.235‡	> 100	0.326‡	7
0.213‡	4	0.324†	3
0.209‡	13	0.318*	3
0.208‡	10	0.276*	7
0.205‡	18	0.257*	8
0.204‡	19	0.252*	11
M 0.202‡	100	0.239‡	10
0.201‡	4	M 0.235*†‡	> 100
0.198‡	4	0.231†	8
0.194‡	3	0.223‡	23
		0.220*†	8
		0.217‡	18
		0.213†‡	23
		0.209‡	6
		0.208*†‡	14
		0.205‡	27
		0.204‡	29
		M 0.202†‡	100
		0.201†‡	13
		0.198*‡	7
		0.187*†	3

*Al_8CeFe_4: a = 0.886 nm, c = 0.508 nm, tetragonal.
†Al_6Fe: a = 0.6492 nm, b = 0.7437 nm, c = 0.8788 nm, orthorhombic.
‡Al_3Fe: a = 4.743 nm, b = 1.545 nm, c = 0.807 nm, orthorhombic.
M = matrix.

Whereas the iron in solid solution will decrease the lattice spacing [10], elements such as cerium will expand the aluminium lattice. The combination of the two types of solutes make the spacings deviate only 0.16% from that of pure aluminium and may, therefore, reflect the reason for a long incubation period for secondary precipitation [5]. We caution also that the lattice spacings given above may be averaging over the two zones and a direct comparison with varying composition will not be strictly correct unless the relative volumes of the two zones is known a priori to X-ray measurement.

TABLE III X-ray diffraction data for alloy II

As-cast		Aged 345° C/312 h	
Observed d (nm)	Relative intensity	Observed d (nm)	Relative intensity
		0.490†	2
M 0.234*	> 100	0.407*	3
		0.328*	3
M 0.203*	100	0.319‡	4
		0.278‡	6
		0.259†	4
		0.253‡	3
		0.240†	6
		M 0.234*‡	> 100
		0.225*†	9
		0.218*	2
		0.214*†	8
		0.208*‡	8
		0.205*	16
		M 0.203*	100
		0.193*	3
		0.189*‡	3

*Al_3Fe: a = 4.743 nm, b = 1.545 nm, c = 0.807 nm, orthorhombic.
†Al_6Fe: a = 0.6492 nm, b = 0.7437 nm, c = 0.8788 nm, orthorhombic.
‡Al_8CeFe_4: a = 0.886 nm, c = 0.508 nm, tetragonal.
M = matrix.

TABLE IV X-ray diffraction data for alloy III

As-cast		Aged 345° C/312 h	
Observed d (nm)	Relative intensity	Observed d (nm)	Relative intensity
0.438†	3	0.405*	7
0.405D*	3	0.395*	6
0.348†	4	0.366*	5
0.239*	10	0.354*	7
M 0.234*	> 100	0.320*	3
0.213*†	4	0.277*	5
0.208*†	4	M 0.234*	> 100
0.205*	12	0.213*	5
M 0.202*†	100	0.209*	10
0.198*	3	0.208*	10
		0.205*	20
		0.204*	21
		M 0.202*	100
		0.198*	6

*Al_3Fe: a = 4.743 nm, b = 1.545 nm, c = 0.807 nm, orthorhombic.
†Al_6Fe: a = 0.6492 nm; b = 0.7437 nm, c = 0.8788 nm, orthorhombic.
M = matrix; D = diffuse.

3.2. TEM of as-cast condition

Rapid solidification of the Al–10 Fe–1.25 MM alloy (alloy I) shows a dispersed phase of 0.1 to 0.3 μm embedded in a cellular matrix of 0.3 to 0.5 μm. The dispersed phase was identified as Al_3Fe [5]. Regions of high and low particle densities are observed and the cell size in the very low particle density region is lower than 0.1 μm. Distribution of (La, Pr) is seen to follow that of cerium at microprobe magnification. Following the suggestion of Sanders *et al.* [12] the dispersed Al_3Fe phase may have been retained during the melting process or could be the primary intermetallic formed during solidification. In any case, the phase acts as a growth centre for epitaxial solidification and its small size indicates it is the latter. In some areas, a wide band of plane front growth can be observed around the Al_3Fe particle. This is shown in Fig. 2a. The grain size

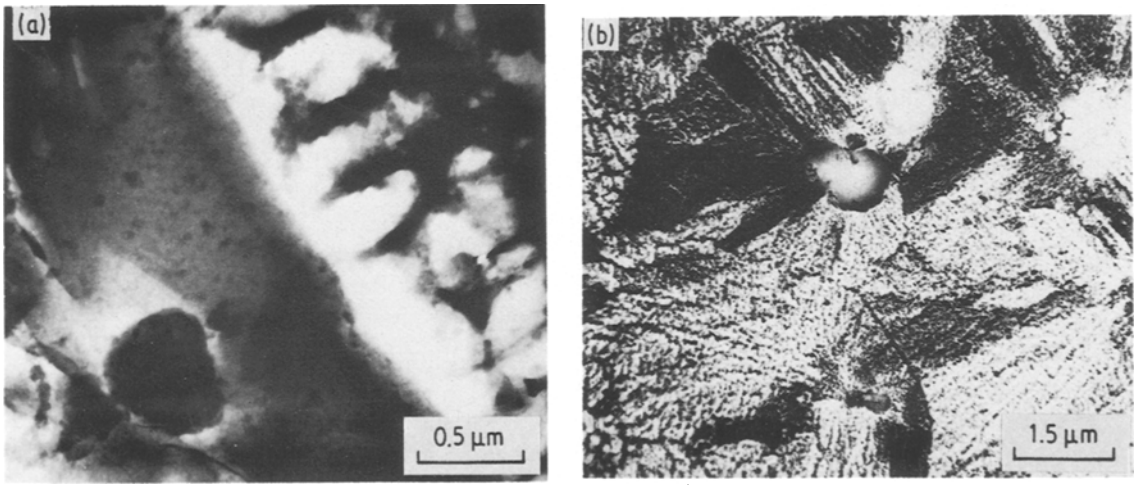

Figure 2 (a) Transmission electron micrograph showing plane front growth around Al_3Fe particle in alloy I (as-cast condition). (b) TEM micrograph showing cellular structure around Al_3Fe precipitate in alloy I. (As-cast condition.)

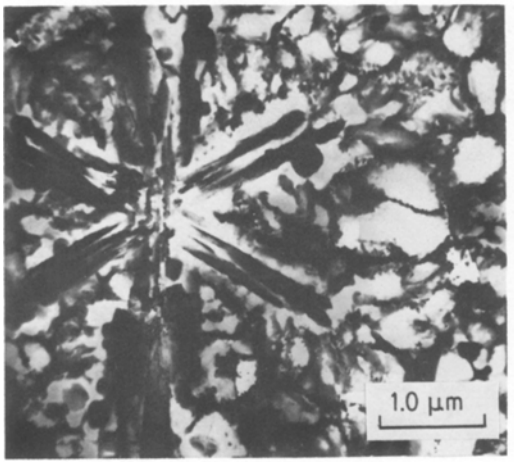

Figure 3 Transmission electron micrograph showing star-like Al_3Fe precipitates in alloy I. (As-cast condition.)

in regions of the type of microstructure shown in Fig. 2b is about 2 to 4 μm. The microstructure spacing adjacent to the Al_3Fe particles in Fig. 2b is extremely fine, of the order of 0.1 μm, in contrast to those reported by Sriram and Sekhar [5] where the cell size was 0.3 μm. The type of microstructure described by the latter authors is also seen and the grain size in these regions is 2 to 4 μm. Additionally, in the coarse cellular region, star-like features are also seen such as those shown in Fig. 3. The stars were identified as Al_3Fe by electron diffraction. Regions where cells are not obvious are shown in Fig. 4. These regions contain very fine precipitates around 0.05 μm in size inside grains of about 1 μm.

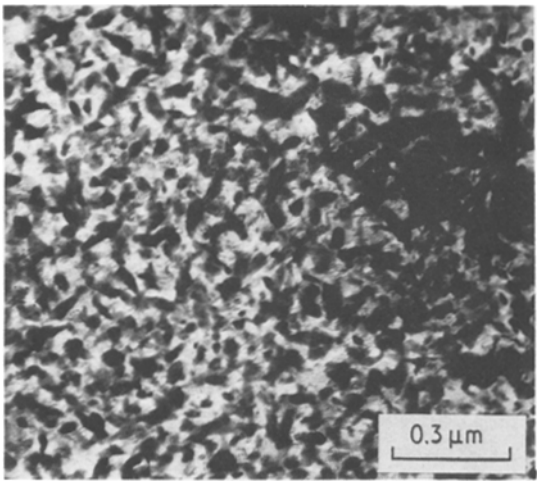

Figure 4 Transmission electron micrograph showing microstructure in another region of the strip corresponding to alloy I. Note that cells are not seen here. (As-cast condition.)

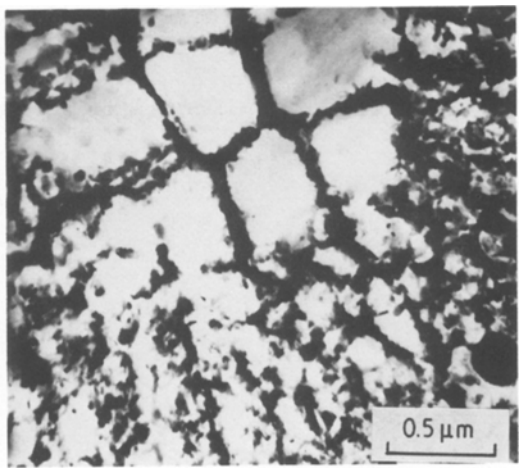

Figure 5 Cellular microstructure in alloy II. (As-cast condition.)

Rapidly solidified Al–6.65 Fe–3.2 MM alloy (alloy II) displays two distinct cell sizes shown in Fig. 5. The larger cell size region contains cells about 0.5 μm thick and the smaller ones are 0.1 μm. The intercellular regions contain precipitates smaller than 0.02 μm. Some needle-like precipitates similar in morphology but about ten times finer than those observed by Jones [10] in chill-cast Al–8 Fe alloys, are also observed. A typical example is shown in Fig. 6a. Although X-ray diffraction did not indicate the presence of any major quantity of Al_3Fe in this alloy, the needle-like structures of Fig. 6a were identified as Al_3Fe. Fig. 6a shows three needles in the same area; however this is not a general phenomena and the needles mostly occur separately in a very sporadic fashion. Figs. 6b and c are the diffraction patterns obtained from the needle marked X. Optical examination of the edge wise strip is shown in Fig. 1. Zones A and B are revealed. Sometimes coarse Al_3Fe needles are seen to form at the edge of zone B when the thickness of the strip exceeded 70 μm.

Rapid solidification of Al–3.6 Fe–1.2 MM alloy (alloy III) displays microstructures showing regions where cells are distinct (Fig. 7a) and where cells do not clearly appear (Fig. 7b). When cells are not clearly seen, there are precipitates somewhat needle-like in morphology and about 0.03 to 0.09 μm in size. A third region, as shown in Fig. 7c, is disturbed cellular or microeutectic with a spacing of about 0.15 μm. No coarse needle-like or star-like precipitates are observed in the microstructure of this alloy.

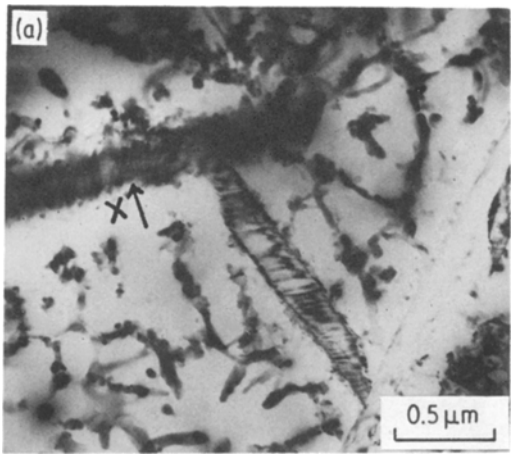

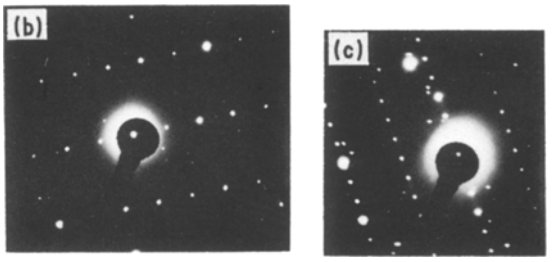

Figure 6 (a) Needle-like Al_3Fe precipitates in alloy II (as-cast condition). (b) SADP from precipitate X orthorhomic zone axis = $(1\bar{2}3)$. (c) SADP from precipitate X orthorhomic zone axis = $(01\bar{3})$.

3.3. Microhardness

Microhardness measurements were carried out for the strips as described by Sriram and Sekhar [5]. The Al–10 Fe–1.25 MM alloy strips heat treated at 618 K (345° C) lead to an initial decrease and a further increase in hardness with heat treatment time [5]. The times were extended to over 300 h during this investigation.

The Vickers microhardness variation (15 g load) along the thickness of the strips when in the cast conditions is shown in Fig. 8a. Even though the strip thickness is about 50 to 80 μm, regions of greater thickness were identified to obtain further sequential data. In all the alloys the hardness of the zone A region is higher than in the zone B region but drops somewhat continuously. Alloy II has the hardest zone A but has a very steep drop in hardness across the strip (Fig. 8a). Fig. 8b shows the hardness variation after heat treating at a temperature of 503 and 618 K for over 300 h. Examining the two sets of curves, alloy II may be a better alloy for use at temperatures such as 503 K but alloy I is harder

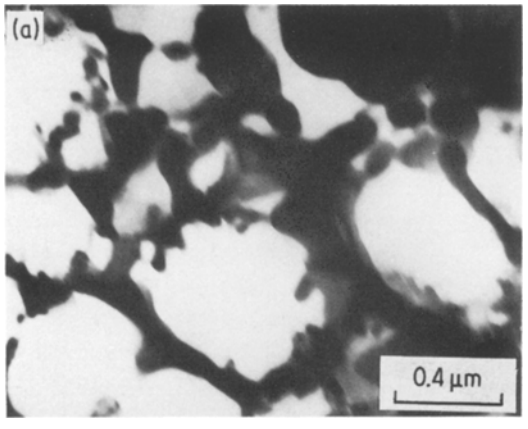

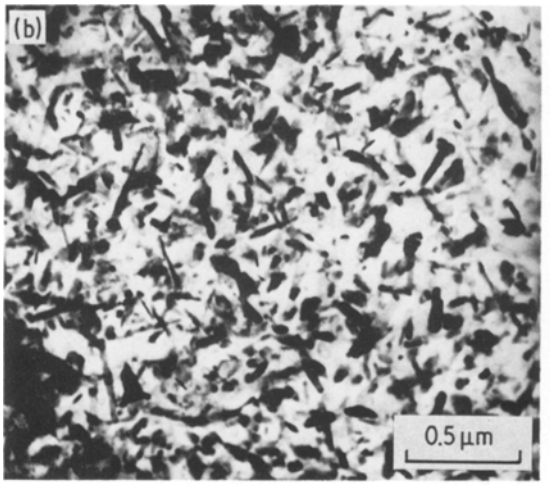

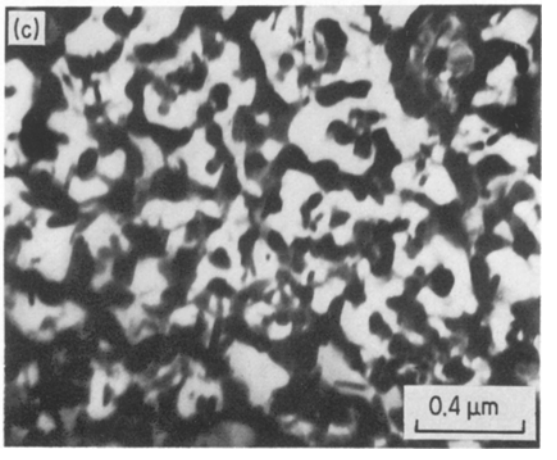

Figure 7 (a) Transmission electron micrograph showing cellular microstructure in alloy III. (b) Transmission electron micrograph showing microstructure in another area of alloy III. (c) Disturbed cellular region in alloy III, transmission electron micrograph. (All in as-cast condition.)

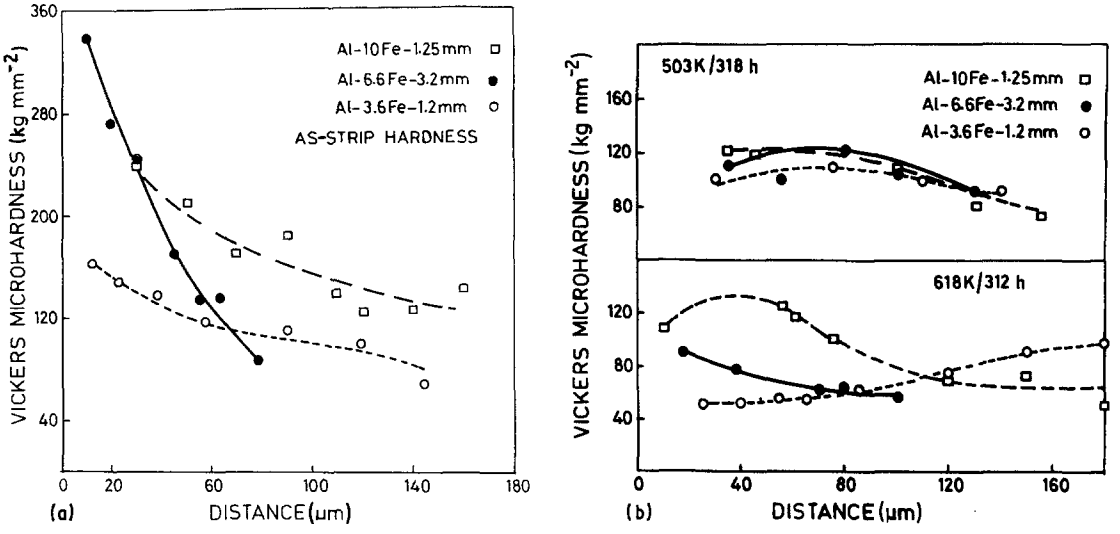

Figure 8 Variation of hardness with distance from substrate-surface of alloys I, II and III in (a) as-cast condition (b) heat treated at 503 K for 318 h and at 618 K for 312 h.

at higher temperatures. This observation is further emphasized on averaging strip hardness over the two faces and edges for various times and temperatures, similar to work reported by Sriram and Sekhar [5]. Tables of these data are given in the Appendix and are a useful compilation to predict the expected strength values from compacts made out of the strips. Alloy III heat treated for 312 h at 618 K (Fig. 8b) shows that for this particular alloy and temperature, zone B is more stable than zone A. The oscillatory behaviour of low and high hardness (Tables A1, A2, A3) with time at any given temperature stems from the varying rates of lattice softening, grain and cell coarsening, precipitation of Al_3Fe and Al_8Fe_4Ce [5] and coarsening of Al_3Fe, Al_6Fe and Al_8Fe_4Ce.

3.4. Heat treated TEM microstructure

Since the as-cast microstructure shows variation from region to region due to zone A, zone B and varied segregation in different regions of the specimen, it is to be expected that these regions will behave differently on heat treatment. The microstructural changes that occur are:

1. coarsening of cells and grains in regions where cells are present;
2. appearance of new phases, more likely in

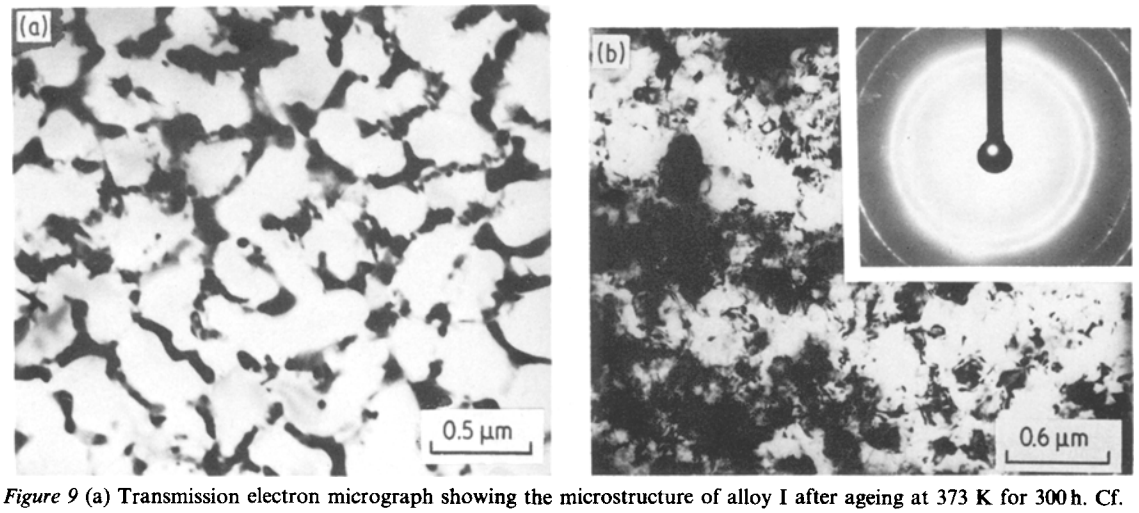

Figure 9 (a) Transmission electron micrograph showing the microstructure of alloy I after ageing at 373 K for 300 h. Cf. microstructure in as-cast condition. (b) Transmission electron micrographs showing fine grains of Al SADP in alloy I, inset showing aluminium rings. Faint rings nearest to centre are from another phase which could not be imaged.

intercellular regions, and their further growth;

3. coarsening of fine precipitates already present in the intercellular region in the fine cellular, disturbed cellular regions and the equiaxed dendrite region;

4. coarsening of precipitates already present in the regions where cells are not evident in the as-strip conditions.

Figs. 9a and b compare the most frequently observed microstructures at 373 K for long times (300 h). Alloys II and III displayed typically similar microstructures showing the cellular structure quite stable at 373 K. In alloy I, needle-like Al_3Fe precipitates are also observed. Fig. 9b shows a typically fine-grained structure observed in all three alloys. SADP from these regions show rings of aluminium with faint outlines of two rings from other phases. This region obviously corresponds to a microcrystalline region which is preserved even on heat treatment.

At higher ageing temperatures, coarsening of cells and the appearance of precipitates in the intercellular region is quite evident in samples aged at 503 K for 96 h and at 618 K for 5 h in all the alloys. Fig. 10 shows a typical region from alloy I after 5 h at 618 K. At 618 K and long heat-treatment times, the Al_6Fe could also, be identified and is shown in Fig. 11. After long ageing times (318 h at 618 K) it is evident that some regions in alloys II and III still show cellular or microeutectic structures (in alloy I a cellular structure is only observed in the region where large Al_3Fe precipitates had been present, Fig. 12). Most of the regions, however, show

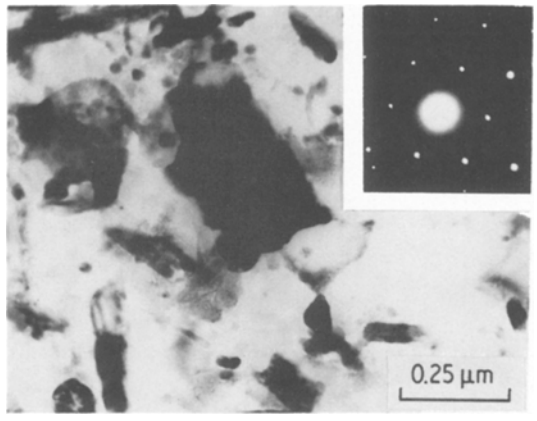

Figure 11 Al_6Fe particle imaged in alloy I after heat treating at 618 K for 312 h. Inset shows the corresponding diffraction pattern. Zone axis = (1 0 1).

two different types of precipitates (Fig. 13) marked A and B, i.e. needle- or plate-like precipitates which were identified as Al_3Fe and oblate precipitates which were found to be tetragonal with $c/a = 0.55$ by electron diffraction. This closely corresponds to Al_8CeFe_4 reported by Sriram and Sekhar [5]. The presence of these two types of precipitates is confirmed by X-ray diffraction. It is to be noted that at 618 K, alloy II has the coarsest precipitate, while the amount of precipitate is larger in alloy I. The relative amount of the Al_8CeFe_4 precipitate is greater in alloy II.

4. Conclusions

1. Examination of the rapidly cast microstructures of the three alloys shows (i) a coarse

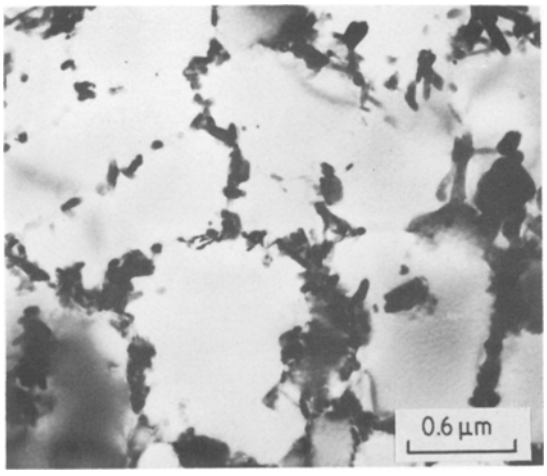

Figure 10 Transmission electron micrograph showing precipitation in intercellular region in alloy I after 5 h at 618 K.

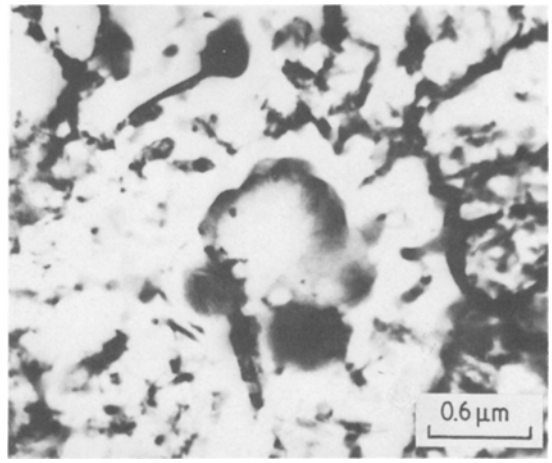

Figure 12 Transmission electron micrograph showing cellular structure around Al_3Fe precipitate in alloy I after 318 h at 618 K.

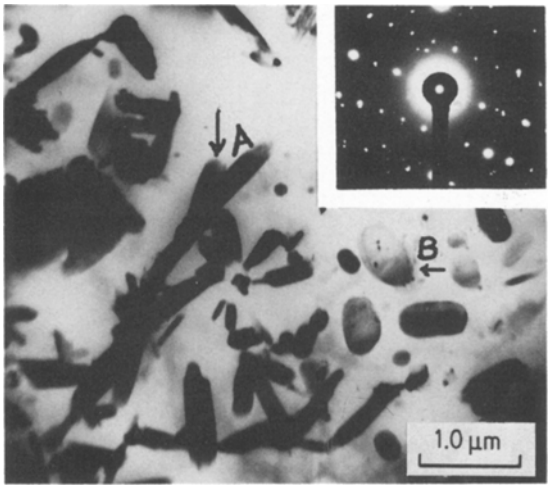

Figure 13 Transmission electron micrographs showing precipitates in alloy II (618 K/318 h). Precipitate marked A is Al_3Fe, that marked B is tetragonal (SADP inset) with $c/a = 0.55$ closely corresponding to Al_8CeFe_4. Zone axis (0 1 0).

cellular region (cell size 0.4 μm), (ii) a fine cellular region (cell size < 0.1 μm), (iii) regions where cells are not visible but small precipitates are evident, and (iv) a microeutectic or disturbed cellular region.

2. Al_3Fe needles are seen in alloy I, much less in alloy II and not at all in alloy III.

3. Alloy II displays a large amount of zone A ($> 50\%$) while alloys I and III show lesser amounts. An increasing amount of misch metal causes an increase in zone A. Alloy II as-cast has very small amounts of the second phase.

4. Lattice constant measurement in the rapidly cast strip condition reveals that the lattice is distorted by less than 0.16% from that of pure aluminium.

5. Heat treatment of the three alloy strips at 618 K for 300 h indicates (i) that in alloy I, Al_6Fe is now present along with Al_3Fe and Al_8Fe_4Ce, (ii) in alloy II, Al_3Fe, Al_6Fe and Al_8Fe_4Ce are now present whereas there was very little of the second phase in the as-cast condition, and (iii) Al_3Fe is the only second phase in alloy III after heat treatment at 618 K/312 h whereas both Al_3Fe and Al_6Fe were indicated in the as-cast condition.

6. Microcrystalline aluminium is stable up to 373 K and some cellular structure is present even after 618 K/318 h treatment.

7. Precipitation at the temperatures studied, occurs mostly at the cellular boundaries.

8. Microhardness values indicate that alloy I is a suitable candidate for operation temperatures of about 600 K whereas alloy II may be a better candidate at 500 K. Alloy III, which shows a stable zone B at elevated temperatures, may be considered for low-strength high-temperature applications of aluminium alloys.

Acknowledgement

The authors thank Dr P. Rama Rao, Director DMRL for encouragement and permission to publish this article.

Appendix

TABLE A1 Vickers microhardness (15 g load) for heat treated strips of Al–10 Fe–1.25 MM alloy (alloy I)

Temperature (° C)	Time (h)	Mean hardness	Standard deviation
As-cast		155	30
100	24	107	22
100	72	148	28
100	96	116	7
100	168	126	14
100	318	134	17
200	5	109	21
230	72	104	4
230	168	116	9
230	240	89	11
230	318	106	15
345	5	106	28
345	24	97	8
345	72	125	18
345	100	137	22
345	312	103	9

TABLE A2 Vickers microhardness (15 g load) for heat treated strips of Al–6.64 Fe–3.2 MM alloy (alloy II)

Temperature (° C)	Time (h)	Mean hardness	Standard deviation
As-cast		185	54
100	72	143	25
100	168	107	13
100	318	139	14
200	5	100	4
200	24	150	29
230	5	166	47
230	72	124	17
230	96	122	19
230	168	119	10
230	318	160	34
345	5	120	20
345	312	87	5

TABLE A3 Vickers microhardness (15 g load) for heat treated strips of Al–3.65 Fe–1.2 MM alloy (alloy III)

Temperature (°C)	Time (h)	Mean hardness	Standard deviation
As-cast		104	12
100	72	88	26
100	96	99	6
100	168	113	11
100	240	155	38
100	318	106	28
200	5	126	18
200	24	104	16
230	5	94	17
230	24	108	14
230	72	102	19
230	96	107	12
230	318	106	12
345	5	105	23
345	312	80	8

References

1. J. P. DURAND, R. M. PELLOUX and N. J. GRANT, *J. Mater. Sci. Eng.* **23** (1976) 247.
2. P. K. DOMALAVAGE, N. J. GRANT and Y. GIFEN, *Met. Trans.* **14A** (1983) 1599.
3. H. G. PARIS, J. W. MULLINS and T. H. B. SANDERS, *Aluminium* **59**(7) (1983) 509.
4. C. M. ADAM and R. G. BOURDEAN, in "RSP-II", edited by R. Mehrabian, B. H. Kear and M. Cohen (Claitor's, Baton Rouge, USA, 1980) p. 246.
5. S. SRIRAM and J. A. SEKHAR, *J. Mater. Sci. Eng. Lett.* **66** (1984) L9.
6. T. H. SANDERS, J. W. JOHNSON and E. E. UNDERWOOD, in "RSP-II", edited by R. Mehrabian, B. H. Kear and M. Cohen (Claitor's, Baton Rouge, USA, 1980) p. 141.
7. K. K. SANKARAN and N. J. GRANT, *J. Mater. Sci. Eng.* **44** (1980) 213.
8. H. JONES, *Aluminium* **54**(4) (1978) 274.
9. G. THURSFIELD and M. J. STOWELL, *J. Mater. Sci.* **9** (1974) 1644.
10. H. JONES, *Mater. Sci. Eng.* **5** (1969/1970) 1.
11. B. VAN DEN BRANDT, P. J. VAN DEN BRINK, H. F. DE JONG and L. KATGERMAN, *J. Mater. Sci. Lett.* **2** (1983) 67.
12. T. H. SANDERS, H. G. PARIS and J. W. MULLINS, in "Rapidly Solidified Amorphous and Crystalline Alloys", edited by B. H. Kear, B. C. Giessen and M. Cohen (Elsevier, New York, 1982) p. 369.
13. P. P. MILLAN, Jr, *J. Metals*, **35**(3) (1983) 76.
14. L. J. MASUR, J. T. BURKE, T. Z. KATTAMIS and M. C. FLEMINGS, in "Rapidly Solidified Amorphous and Crystalline Alloys", edited by B. H. Kear, B. C. Giessen and M. Cohen (Elsevier, New York, 1982) p. 185.
15. J. A. SEKHAR and T. CHANDE, *Trans. IIM* **37**(1) (1984) 67.
16. R. K. GARRETT and T. H. SANDERS, *Mater. Sci. Eng.* **60** (1983) 269.
17. H. JONES, in "RSP II", edited by R. Mehrabian, B. H. Kear and M. Cohen (Claitor's, Baton Rouge, USA, 1980) p. 306.
18. C. McLADAM in "Insitu composites III", edited by J. L. Walter, M. F. Gigliote, B. F. Oliver and H. Bibring (GINN Custom Publishing, Massachusetts, 1979) p. 36.
19. I. R. HUGHES and H. JONES, *J. Mater. Sci.* **12** (1977) 323.
20. M. H. JACOBS, A. G. DOGGEST and M. J. STOWELL, *ibid.* **9** (1974) 1631.
21. J. A. SEKHAR, *Trans. IIM* (1985) to be published.

Received 6 June
and accepted 20 September 1984